5

Vehicle suspension control

5.1 Introduction

This chapter describes the development and validation of the multi-electromagnet vehicle suspension control strategy outlined at the end of Chapter 1. The suspension controller developed in Chapter 4 is used to control independent vehicle modes, and the force controller developed in Chapter 3 is used to provide independent electromagnet force actuation.

The development of the vehicle control system is divided into six parts. First, the characteristics of the vehicle chassis and guideway are identified. The decoupling and control requirements are then considered and a vehicle suspension control strategy is developed. Next, the control system is synthesised using the independent force and suspension controllers developed in Chapters 3 and 4 respectively. The lateral motion of the vehicle is then briefly analysed. Experimental test results are presented next, to verify that the proposed vehicle suspension system meets the operational requirements. Finally, some conclusions are drawn on the merits and limitations of the proposed system.

5.2 The experimental research vehicle and guideway

The chassis of the experimental research vehicle is designed to be very stiff in order to provide a rigid coupling between the electromagnets and this exacerbates the problems of controlling the vehicle.[76] Figure 5.1 shows a photograph of the experimental vehicle and its guideway. The vehicle is suspended by four electromagnets, one at each corner, and is propelled and braked by a linear induction motor mounted centrally

underneath the chassis. The vehicle is equipped with all of the signal processing and power control equipment necessary to implement the proposed control schemes.

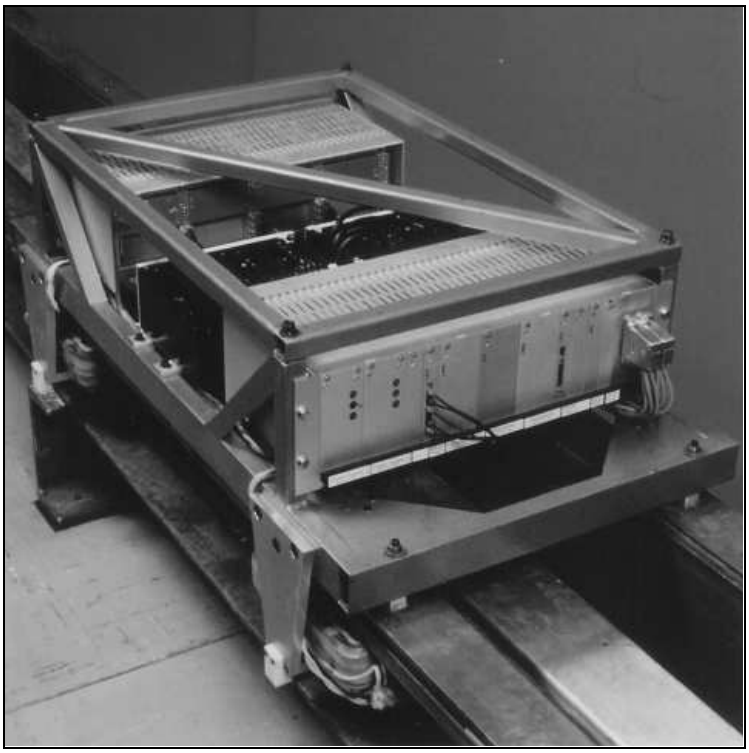

Figure 5.1 Vehicle chassis

The chassis is constructed from welded steel tubing, with an aluminium alloy used for the electromagnet hangers to prevent conduction of the electromagnet flux. The torsional stiffness of the chassis, measured axially about the length of the vehicle is about 112 kNm/rad. The flexibility of the electromagnet support hangers gives rise to a coupling stiffness of about 1.5 kN/mm between each electromagnet pole face and the vehicle chassis. The chassis is assumed to be rigid apart from the torsional and electromagnet hanger flexibility.

The experimental electromagnets and reaction rail are too narrow to permit direct measurement of the electromagnet air gap. Therefore, the gap sensors measure the distance from the chassis down to the top of the track, and the electromagnet air gaps are calculated using an appropriate formula. This arrangement is not ideal due to the flexibility of the electromagnet hangers which introduces small errors in the air gap measurement. In order to limit the magnitude of such errors, the air gap sensors are calibrated with a preloaded mass of 35 kg per electromagnet. A suspended mass of 20-50 kg per electromagnet thus gives rise to a maximum measurement error of ±0.1 mm due to steady-state hanger deflection. The accelerometers are rigidly mounted

to the underside of the electromagnets and are therefore assumed to be perfectly coupled.

The guideway is constructed from stiff steel girders which carry ferromagnetic reaction rails for the electromagnets and a steel-backed, aluminium alloy reaction rail for the linear motor. When excited with a force impulse, the guideway exhibits lightly damped oscillation modes at natural frequencies of around 20 Hz and 40 Hz.

The mass of the fully equipped vehicle is 88 kg which permits a maximum passenger load of about 110 kg. Table 5.1 lists the mass of each of the major vehicle components and the dimensions between the centres of the electromagnets. The linear motor which propels the vehicle produces a maximum thrust of about 50 N and an associated repulsion force of around 200 N.

Table 5.1 Component masses and dimensions of the experimental vehicle

Vehicle parameter	Index	Size
Chassis Mass	$m_{chassis}$	27 kg
Total Electromagnet Mass	$m_{magnets}$	29 kg
Linear Induction Motor Mass	m_{LIM}	14 kg
Control System Equipment Mass	$m_{control}$	18 kg
Total Vehicle Mass	m	88 kg
Chassis length (between electromagnet centres)	L	0.8 m
Chassis width (between electromagnet centres)	W	0.4 m

5.3 Control strategy for the vehicle suspension

The free-body motion of the vehicle has six degrees of freedom which can be considered in terms of three cartesian modes of linear motion, namely, heave, sway and track progress, and the three corresponding cartesian rotation modes, pitch, roll and yaw. These modes are illustrated in Figure 5.2, along with the electromagnet indices.

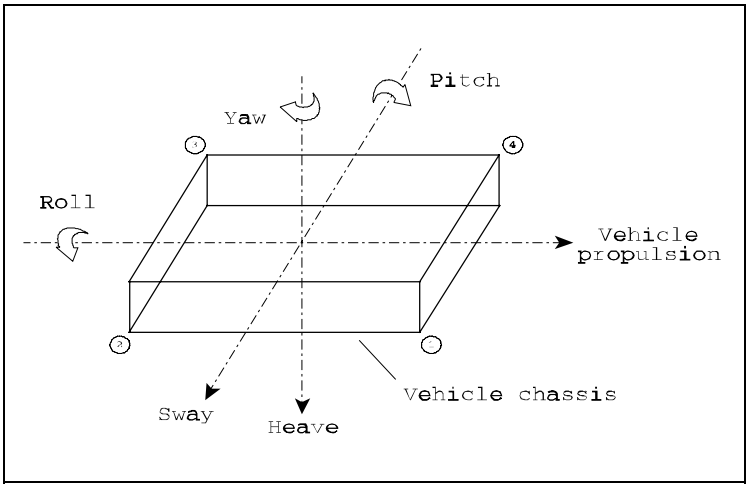

Figure 5.2 Free-body motion of the vehicle

The experimental vehicle has no provision for active lateral force actuation, so the sway and yaw modes are not actively controlled. Lateral guidance is, however, provided by the inherent lateral stiffness which exists between the suspension electromagnets and the reaction rails, whilst the progress of the vehicle along the guideway is controlled by the linear induction motor. The four lift suspension electromagnets on the experimental vehicle therefore control three free-body motions, namely, heave, pitch and roll. The redundancy associated with four electromagnets controlling only three free-body motions, results in the control of a fourth degree of freedom, namely, torsional distortion of the vehicle chassis.

The suspension requirements for the independent vehicle modes are functionally equivalent to those identified in Chapter 4, but different suspension parameters are required for the different vehicle modes. For example, in order to maintain the correct nominal air gaps, and hence maximise the available air gap deviation range, the heave, pitch and roll modes require position error integral action. However, an important operational requirement for an electromagnetically suspended vehicle is for the suspension forces to be evenly distributed among the electromagnets. This is required because suspension electromagnets are designed with only a moderate overload capability due to the weight penalty that it incurs (see Appendix A). Since a cost effective vehicle and guideway configuration will always have some finite torsional displacement error, the application of torsional position error integral action would cause a severe load imbalance between diagonal pairs of electromagnets. This would clearly be unsatisfactory from an electromagnet utilisation viewpoint. The application of position error integral action to the vehicle torsion motion is thus precluded. For full-scale vehicles, it may also be desirable to have different settings for the heave,

pitch and roll mode suspensions,[77,78] as is found on conventional trains and road vehicles.

Since the required suspension characteristics for the vehicle modes differ, independent vehicle mode suspension controllers are required.[79,80] The proposed vehicle control strategy therefore employs the suspension control algorithm developed in Chapter 4 to control independently each of the vehicle modes, heave, pitch, roll and torsion. Figure 5.3 shows the configuration of the proposed vehicle suspension control strategy, where C, Z and F represent air gaps, accelerations and forces/torques respectively. The electromagnet feedback signals for air gap and acceleration are first transformed to vehicle mode coordinates and then fed into independent mode suspension controllers. The force and torque demands from the suspension controllers are then transformed to electromagnet force demands. The electromagnet force controller proposed and developed in Chapter 3 is then used to achieve independent electromagnet force actuation. The synthesis of the proposed vehicle control strategy is described next.

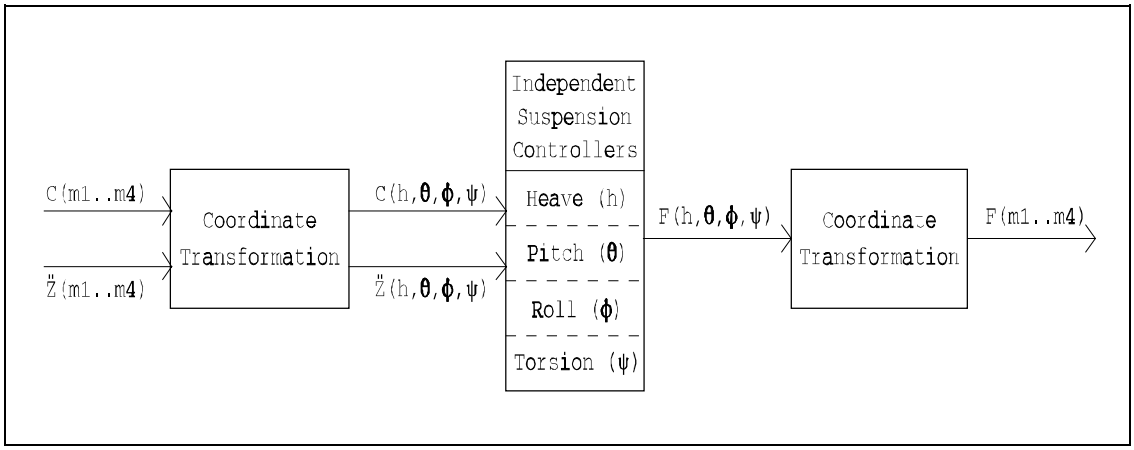

Figure 5.3 Configuration of the vehicle suspension control system

5.4 Synthesis of the vehicle control system

The synthesis of the vehicle suspension control system is performed in three stages. First, the transformations required to convert the electromagnet coordinate signals to and from vehicle mode coordinates are identified. Then, for convenience of design, the vehicle mode angular measurements are normalised so that they are equivalent to the linear motions which they generate at the electromagnets. This is achieved by reformulation of the decoupling transformations, and conversion of the vehicle mode inertias. Finally, the parameters of the suspension control algorithm developed in the previous chapter are configured for each vehicle mode.

5.4.1 Decoupling the electromagnet motions

The maximum angular displacement of any vehicle motion is less than 1°. Therefore, the vehicle mode motions (see Figure 5.2) can be accurately approximated by Equation 5.1 where h, θ, ϕ and ψ are the positions of the vehicle modes, heave, pitch, roll and torsion respectively, z_{m1}-z_{m4} are the positions of the electromagnets, and L and W are the vehicle length and width measured between the electromagnet centres (see Table 5.1).

$$\begin{bmatrix} h \\ \theta \\ \phi \\ \psi \end{bmatrix} \approx \frac{1}{4} \begin{bmatrix} +1 & +1 & +1 & +1 \\ +2/L & -2/L & -2/L & +2/L \\ +2/W & +2/W & -2/W & -2/W \\ +2/W & -2/W & +2/W & -2/W \end{bmatrix} \begin{bmatrix} z_{m1} \\ z_{m2} \\ z_{m3} \\ z_{m4} \end{bmatrix} \qquad \textbf{5.1}$$

The corresponding transformation between vehicle mode forces and torques, and the electromagnet forces is given by Equation 5.2. This transformation matrix reflects the additive nature of force and torque translations, compared with the averaging nature of displacement translations.

$$\begin{bmatrix} F_{m1} \\ F_{m2} \\ F_{m3} \\ F_{m4} \end{bmatrix} \approx \frac{1}{4} \begin{bmatrix} +1 & +2/L & +2/W & +2/W \\ +1 & -2/L & +2/W & -2/W \\ +1 & -2/L & -2/W & +2/W \\ +1 & +2/L & -2/W & -2/W \end{bmatrix} \begin{bmatrix} F_h \\ T_\theta \\ T_\phi \\ T_\psi \end{bmatrix} \qquad \textbf{5.2}$$

The masses of the major components from which the vehicle is constructed are listed in Table 5.1. In order to determine the contribution of each of these masses to the inertia of the rotational vehicle modes, the distribution of the mass of each component in a horizontal plane is considered. The heights of the component masses relative to a horizontal reference plane are considered later.

The centres of gravity of each electromagnet and the induction motor are assumed to be located at their respective centres of geometry. The electromagnets are located at the four corners of the rectangular chassis, whilst the motor is located at the geometric centre of the chassis. The mass of the chassis is concentrated around its periphery, so

it is modelled by four point masses, located at the electromagnet centres, with each point mass equal to one quarter of the total chassis mass.

The mass of the control system electronics is distributed fairly uniformly over the rectangular space between the electromagnets. It is therefore modelled by four point masses, each of one quarter of the total electronics mass, which are located mid-way between each electromagnet and the geometric centre of the chassis. Equation 5.3 shows the contribution of each component mass to the mass or inertia of each vehicle mode. The resultant mass and inertias are calculated using the masses and dimensions given in Table 5.1.

$$\begin{bmatrix} m_h \\ I_\theta \\ I_\phi \\ I_\psi \end{bmatrix} \approx \begin{bmatrix} 1 & 1 & 1 & 1 \\ (L/2)^2 & (L/2)^2 & (L/4)^2 & 0 \\ (W/2)^2 & (W/2)^2 & (W/4)^2 & 0 \\ (W/2)^2 & (W/2)^2 & (W/8)^2 & 0 \end{bmatrix} \begin{bmatrix} m_{chassis} \\ m_{magnets} \\ m_{control} \\ m_{LIM} \end{bmatrix} = \begin{bmatrix} 88\ kg \\ 9.7\ kgm^2 \\ 2.4\ kgm^2 \\ 2.3\ kgm^2 \end{bmatrix} \qquad \textbf{5.3}$$

5.4.2 Normalising the vehicle mode motions

For the sake of convenience in considering the design parameters for the vehicle mode controllers, the rotational vehicle mode motions are normalised so that they are equivalent to the linear motions which they produce at the electromagnets. The reformulated transformations are given by Equations 5.4 and 5.5.

$$\begin{bmatrix} z_h \\ z_p \\ z_r \\ z_t \end{bmatrix} \approx \frac{1}{4} \begin{bmatrix} +1 & +1 & +1 & +1 \\ +1 & -1 & -1 & +1 \\ +1 & +1 & -1 & -1 \\ +1 & -1 & +1 & -1 \end{bmatrix} \begin{bmatrix} z_{m1} \\ z_{m2} \\ z_{m3} \\ z_{m4} \end{bmatrix} \qquad \textbf{5.4}$$

$$where \quad z_p = \frac{L\theta}{2}, \quad z_r = \frac{W\phi}{2}, \quad z_t = \frac{W\psi}{2}$$

In a similar fashion, the inertia of each vehicle mode is normalised so that it is equivalent to a point mass at the electromagnet centres. Equation 5.6 shows the normalised mode masses reformulated from Equation 5.3. The angular torsional stiffness of the vehicle chassis is also normalised using the factors in Equations 5.4 and 5.5 giving an equivalent linear stiffness of 1400 N/mm.

$$\begin{bmatrix} F_{m1} \\ F_{m2} \\ F_{m3} \\ F_{m4} \end{bmatrix} \approx \frac{1}{4} \begin{bmatrix} +1 & +1 & +1 & +1 \\ +1 & -1 & +1 & -1 \\ +1 & -1 & -1 & +1 \\ +1 & +1 & -1 & -1 \end{bmatrix} \begin{bmatrix} F_h \\ F_p \\ F_r \\ F_t \end{bmatrix} \qquad \textbf{5.5}$$

$$where \quad F_p = \frac{2T_\theta}{L}, \quad F_r = \frac{2T_\phi}{W}, \quad F_t = \frac{2T_\psi}{W}$$

$$\begin{bmatrix} m_h \\ m_\theta \\ m_\phi \\ m_\psi \end{bmatrix} \approx \begin{bmatrix} 1 & 1 & 1 & 1 \\ 1 & 1 & 1/4 & 0 \\ 1 & 1 & 1/4 & 0 \\ 1 & 1 & 1/16 & 0 \end{bmatrix} \begin{bmatrix} m_{chassis} \\ m_{magnets} \\ m_{control} \\ m_{LIM} \end{bmatrix} = \begin{bmatrix} 88\ kg \\ 61\ kg \\ 61\ kg \\ 57\ kg \end{bmatrix} \qquad \textbf{5.6}$$

$$where \quad m_\theta = \frac{4I_\theta}{L^2}, \quad m_\phi = \frac{4I_\phi}{W^2}, \quad m_\psi = \frac{4I_\psi}{W^2}$$

5.4.3 Control of the vehicle mode motions

The centre of mass of the vehicle lies centrally above the horizontal plane linking the accelerometers which are used to derive the position feedback signals. The pitch and roll modes are therefore coupled to the heave mode.[81] Since the height of the centre of mass of the vehicle above the accelerometer plane is much smaller than the vehicle length or width, the degree of mode coupling is low. The vehicle mass distribution causes negligible cross-coupling between the pitch and roll modes, and from the heave mode to the pitch and roll modes. Since the amount of vehicle mode cross-coupling is small, decoupling is considered unnecessary, and the suspension controllers are applied directly to the vehicle mode motions.

5.4.4 Configuration of the vehicle mode suspension controllers

The functional requirements for the vehicle suspension system are equivalent to those discussed in Section 4.1. The first requirement is that the suspension should deflect no more than 30-50% of the maximum allowable air gap deviation, when subjected to a disturbance or load force equal to 30-50% of the maximum suspended weight. The second requirement is for a peak acceleration of less than 0.04 g, when negotiating a

1 mm step in track height. In addition, in order to maximise the available air gap deviation, there must be no steady-state air gap deflection due to disturbance or load forces for the heave, pitch and roll modes.

The suspension control algorithm developed in Chapter 4 is now configured for each of the vehicle modes. The electromagnets are rated for a maximum continuous force of 500 N, so the maximum suspension force for the vehicle is 2000 N. Therefore, in order to meet the disturbance force rejection requirement at any point on the chassis, the heave, pitch and roll mode position controllers require a stiffness of 1000 N/mm. In addition, in order to meet the deflection requirement with the disturbance force equally divided between two diagonally opposed corners of the vehicle, the torsion motion also needs a stiffness of 1000 N/mm. Since the chassis has an inherent damped torsional stiffness of 1400 N/mm, active suspension stiffness for the torsion mode is not required.

The stiffness of each electromagnet hanger is approximately 1500 N/mm which translates to a vehicle mode hanger stiffness of 6000 N/mm since the hangers operate in parallel. This is much larger than the stiffness required for the vehicle mode position controllers, and it is therefore neglected when designing the suspension controllers.

The design procedure for the position controller described in Section 4.4 is applied for the vehicle heave, pitch and roll modes. The design procedure uses as its starting point, the mode stiffnesses determined above, the chassis mode masses calculated in Equation 5.6, and the maximum passenger load of 110 kg. For the purpose of mode position controller synthesis, the heave mode is conservatively assumed to have the same minimum mass as the other modes. The linearity of the suspension control algorithm and its design procedure, results in vehicle mode feedback gains that are four times the size of those for the single electromagnet suspension design. Table 5.2 lists the parameters for the heave, pitch and roll mode position controllers.

The natural frequencies of the various vehicle modes and components are now considered to check for any potential resonance problems. The predicted closed-loop suspension poles for the vehicle heave, pitch and roll modes are essentially the same as those for the single electromagnet suspension, with a resultant position controller bandwidth of around 10 Hz (see Table 4.4). By assuming a dominantly linear, second-order behaviour for the vehicle torsion motion, its estimated undamped natural frequency[82] is given by:

Table 5.2 Parameters for the heave, pitch and roll mode position controllers.

Parameter	Feedback signal	Value
Stiffness	Position error	1000 N/mm
Damping	Velocity	26 N/mm/s
Virtual mass	Acceleration	60 kg
Integral time constant	Position error integral	1 s

$$\omega_{torsion} = \sqrt{\frac{k_{torsion}}{m_{torsion}}} = \sqrt{\frac{1400000}{57}} \approx 157\ rad/s, \quad f_{torsion} \approx 25\ Hz \qquad \textbf{5.7}$$

Similarly, the estimated undamped natural frequency of each electromagnet and hanger is given by:

$$\omega_{hanger} = \sqrt{\frac{k_{hanger}}{m_{hanger}}} = \sqrt{\frac{1500000}{7.5}} \approx 450\ rad/s, \quad f_{hanger} \approx 71\ Hz \qquad \textbf{5.8}$$

The predicted natural frequency of the electromagnet hangers is well separated from the design values for the vehicle heave, pitch, roll and torsion modes, so problems of resonant coupling are unlikely to occur. However, one of the guideway resonance modes has a natural frequency of around 20 Hz which is likely to interact with the torsion mode. In view of this fact, and the open-loop unstable nature of the electromagnetic force actuators, the use of velocity and acceleration feedback for the torsion mode is considered prudent.

Therefore, the damping of each electromagnet is made equivalent to that of the independent electromagnet suspension of Chapter 4 by using the same velocity feedback gain for the torsion mode as is used for the other mode controllers. The same argument is applied to the acceleration feedback.

The remaining vehicle suspension system design parameters are the corner frequencies for the guideway following filters and state integration filters, and the force actuation time constant. For the vehicle mode suspensions, these are 4 Hz, 0.1 Hz and 3.2 ms

respectively, which are the same as those for the single electromagnet suspension due to the linearity of the position control algorithm and design procedure. Table 5.3 summarises the parameters for the full vehicle suspension control system.

Table 5.3 Parameters for the vehicle mode suspension controllers

Parameter	Name	Value
Stiffness*	k_{pos}	1000 N/mm
Damping	k_{vel}	26 N/(mm/s)
Virtual mass	k_{acc}	60 kg
Error integral time constant*	T_{err}	1 s
Force actuation time constant	T_{force}	3.2 ms
State integration filter frequency	ω_{int}	0.6 rad/s
Guideway following frequency	ω_{follow}	25 rad/s

* For the torsion mode suspension controller: k_{pos} = 0 N/mm, T_{err} = ∞ s.

5.5 Lateral vehicle guidance

The inherent lateral stiffness of the electromagnets provides guidance forces for the vehicle sway and yaw motions. The undamped natural frequency of the lateral motion is derived for small lateral perturbations of the electromagnets in Chapter 4, and is repeated here for convenience. It is approximated by:

$$\omega_n \approx \sqrt{\frac{2 m_t a_g}{m_c \pi p}} \qquad \textbf{5.9}$$

where ω_n is the undamped natural frequency, m_t is the total suspended mass, m_c is the rigidly coupled suspended mass, a_g is gravitational acceleration, and p is the width of the electromagnet pole pieces. The mass ratio m_t/m_c is unity for the unloaded vehicle, and approximately 2 when carrying a passenger. Since the pole width is 9.5 mm, the undamped natural mode frequencies are around 4 Hz for the unloaded vehicle, and 6 Hz for the vehicle supporting a passenger. The lateral guidance thus experiences a second-order guideway following characteristic with a bandwidth very similar to that

of the actively controlled vertical modes, but without the high absolute position stiffness.

5.6 Performance of the experimental vehicle suspension

In order to verify that the proposed vehicle suspension control system is capable of meeting the desired suspension performance, an experimental vehicle was developed, and experimental test results were obtained. The configuration and parameters of the vehicle control system are described earlier in this chapter, whilst the suspension control algorithm and electromagnet force control algorithm are described in Chapters 4 and 3 respectively. The implementation of the hardware and software for the experimental vehicle is described in Chapter 6.

The performance of the experimental vehicle is tested in three phases. The first phase tests the mode position controllers by examining the reference position step response, the disturbance force rejection response, and the stability margins. The second phase tests the degree of cross-coupling between the vehicle mode motions and examines the load sharing performance. Finally, the third phase tests the suspension ride quality when subjected to simulated track steps.

Selected tests were performed with the vehicle both stationary and in motion, and no significant response differences were observed between the two cases.

5.6.1 Performance and stability of the mode position controllers

The performance of the vehicle mode position controllers is tested by analysing the reference position step response and the force disturbance step response. The stability margins are then measured by examining the response in the frequency domain using a Bode plot.[83] In addition, a series of position step responses at different air gaps is presented to gauge the linearity of the suspension control system over the full operational air gap range.

The position step response of the vehicle heave mode controller for a 1 mm reference step amplitude is shown in Figure 5.4 for the unladen vehicle, and in Figure 5.5 for the vehicle with an 80 kg passenger. The transient air gap response should be equivalent to the simulated and experimental responses for the single electromagnet suspension

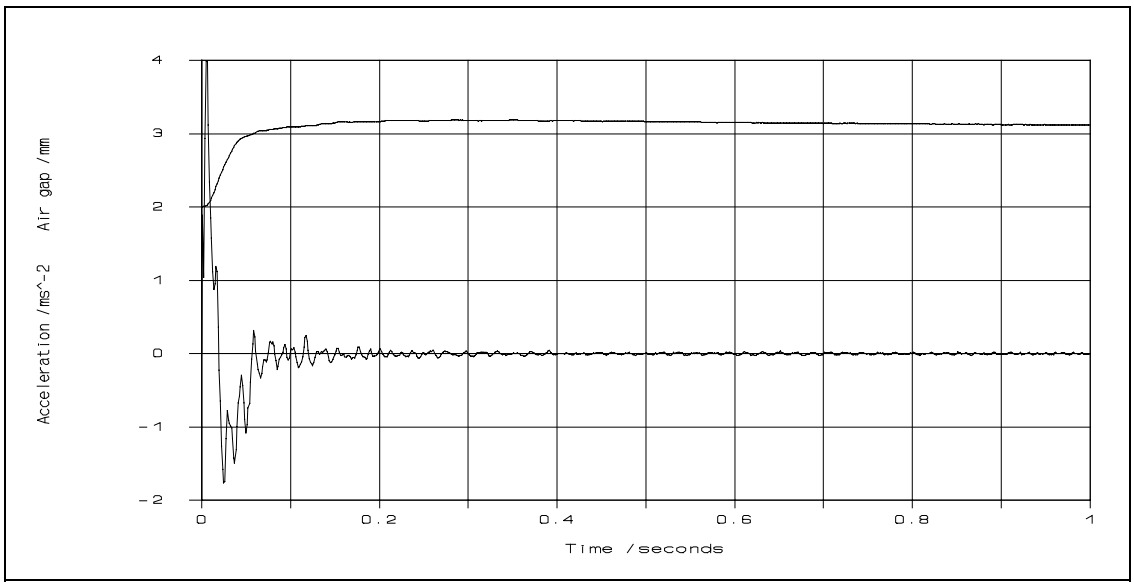

Figure 5.4 Experimental heave response to a 1 mm position reference step (no passenger)

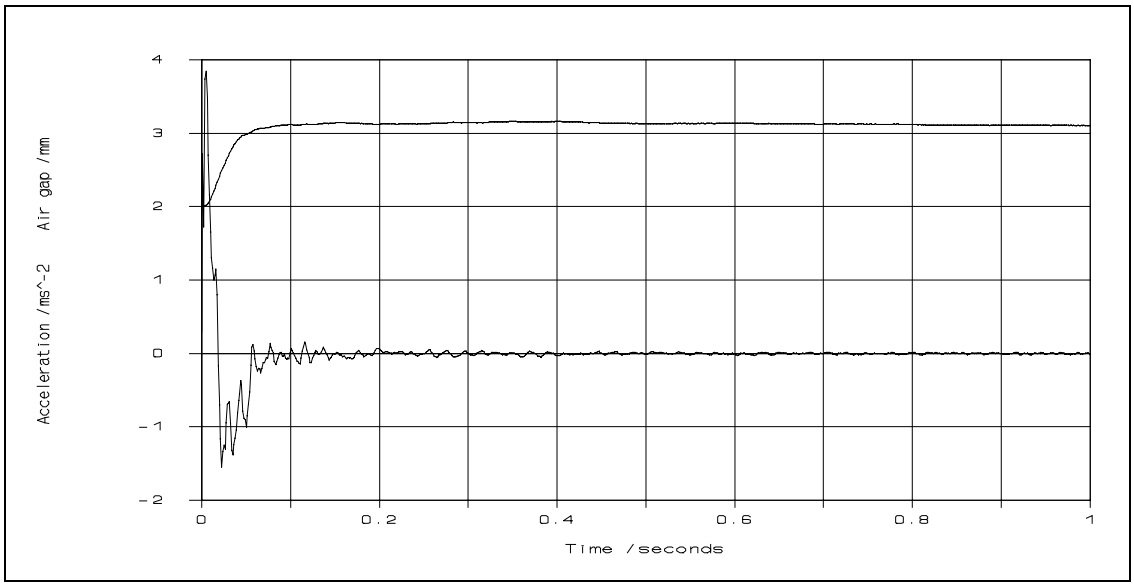

Figure 5.5 Experimental heave response to a 1 mm position reference step (80 kg passenger)

presented in Chapter 4 (see Figures 4.6 and 4.7). The 50% rise time for the vehicle is about 10% smaller than that for the single electromagnet suspension, but the responses are otherwise consistent. The oscillation present on the acceleration signal has a frequency of just under 70 Hz and is attributed to the electromagnet hangers which have an estimated undamped natural frequency of 71 Hz (see Equation 5.8). The low frequency overshoot after the transient part of the response has a peak value of 15%. This is due mostly to the a.c. coupling of the absolute feedback signals, which causes reduced position and velocity signal amplitudes at low frequencies (see Section 4.4.6). Some of the overshoot is also contributed by the position error integral action adjusting

to the new force actuation error that results from the change in electromagnet operating point.

Since the passenger mass is loosely coupled to the vehicle at the frequencies encountered in the transient portion of the step response, the loaded and unloaded responses are very similar. The consistency between the unloaded and loaded responses also shows that the mode force actuation is dominantly linear over a wide force actuation range.

A critical performance requirement for the vehicle suspension is disturbance force rejection. This is tested by measuring the deflection when starting and stopping the linear induction motor and when adding and removing a 500 N load. The induction motor produces a lift force of about 200 N at a thrust of 40 N which causes the vehicle to rise and fall transiently by 0.22 mm. This corresponds well with the theoretical value of 0.2 mm due to the heave mode stiffness of 1000 N/mm. Operation of the linear motor has a negligible impact on the heave mode position step response.

Figure 5.6 shows the air gap and acceleration response to a 50 kg vehicle load reduction. This produces a deflection of 0.61 mm which again corresponds well with the theoretical value of 0.5 mm. For both test cases, the disturbance response is well damped with the position error integral feedback restoring the reference air gap in about 2 seconds.

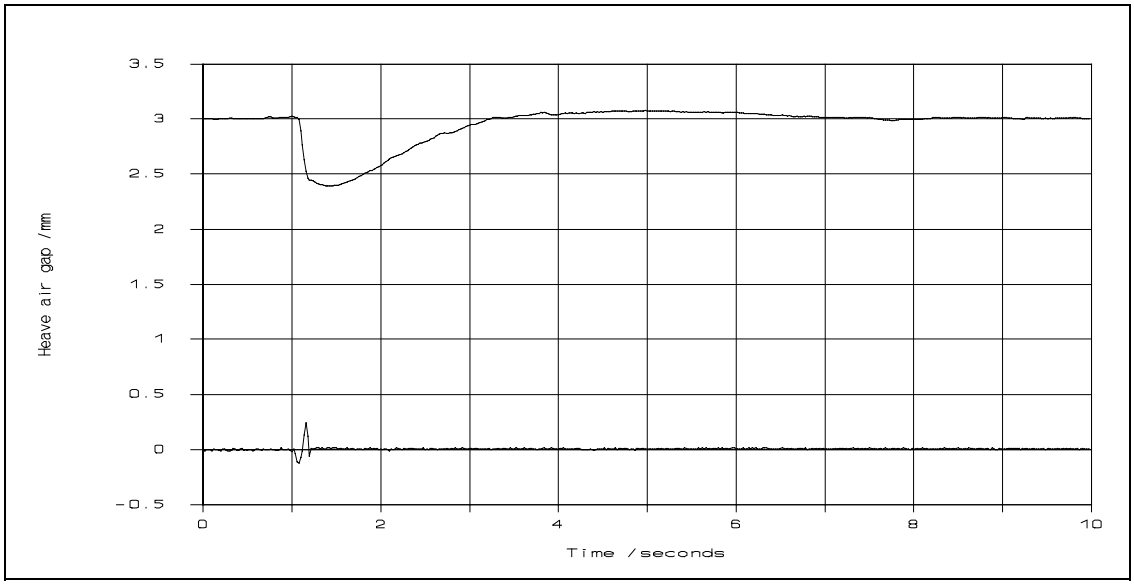

Figure 5.6 Experimental heave response to a 500 N heave disturbance force

The air gap linearity of the mode suspensions is tested by comparing position step responses at different air gaps. Figure 5.7 shows three position step responses for the heave mode position controller. The response of each step is essentially the same, although there is a slight variation in the overshoot recovery characteristic. The latter effect is most notable at the small and large air gaps because the electromagnet force controllers are less accurate near the operational air gap limits than they are around the nominal operational air gap. However, the step responses show that the suspension is dominantly linear over the full operational air gap range.

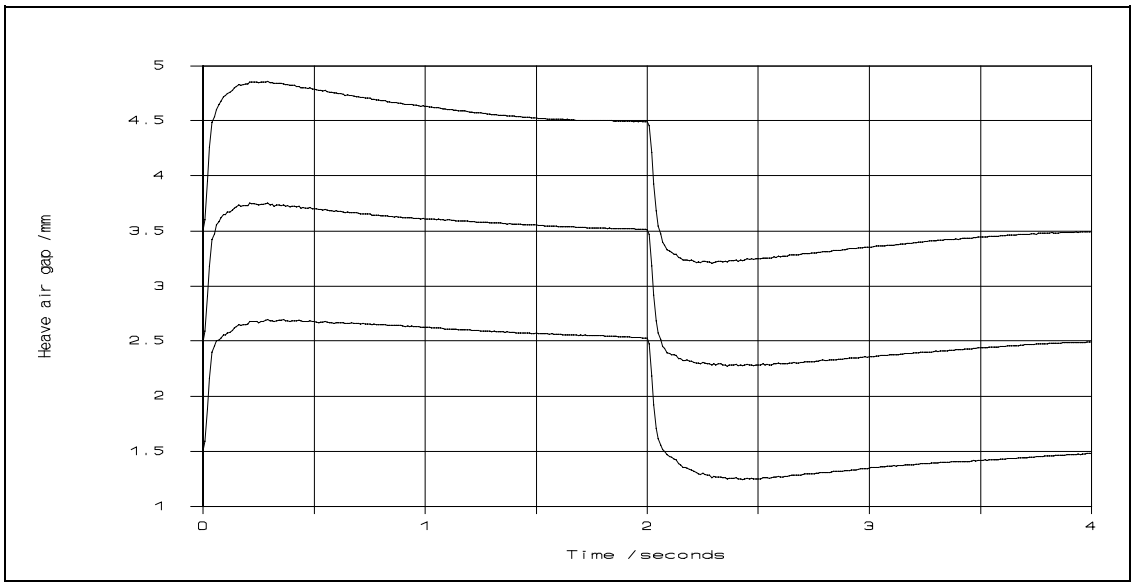

Figure 5.7 Experimental heave responses to three 1 mm heave position reference steps

For the suspension stability analysis in the frequency domain, the worst case scenario is represented by the heave mode controller. The larger mass for the heave mode relative to the equivalent masses of the pitch and roll modes gives the heave mode a slightly lower damping ratio. Figure 5.8 and Figure 5.9 show the theoretical and experimental Bode plots for the position response of the vehicle heave mode controller for a 1 mm amplitude sinusoidal position reference. The theoretical plots are calculated using Equation 4.8 which neglects the low frequency effects due to the state integration filters and the position error integral action. In addition, no allowance is made for the closed-loop phase delay which is generated by the discrete-time controller. For example, the average signal processing time delay of 1.6 ms (see Section 6.5.5) causes an effective feedback loop phase delay of 37° at a frequency 64 Hz.

As with the time domain responses, only a small difference was observed between the Bode plots for the unloaded and passenger loaded vehicle due to the relatively flexible coupling of the passenger body to the vehicle. The signal magnification at low

frequencies is due to the low frequency gain roll-off of the state integration filters which are used to calculate the absolute velocity and position feedback signals.

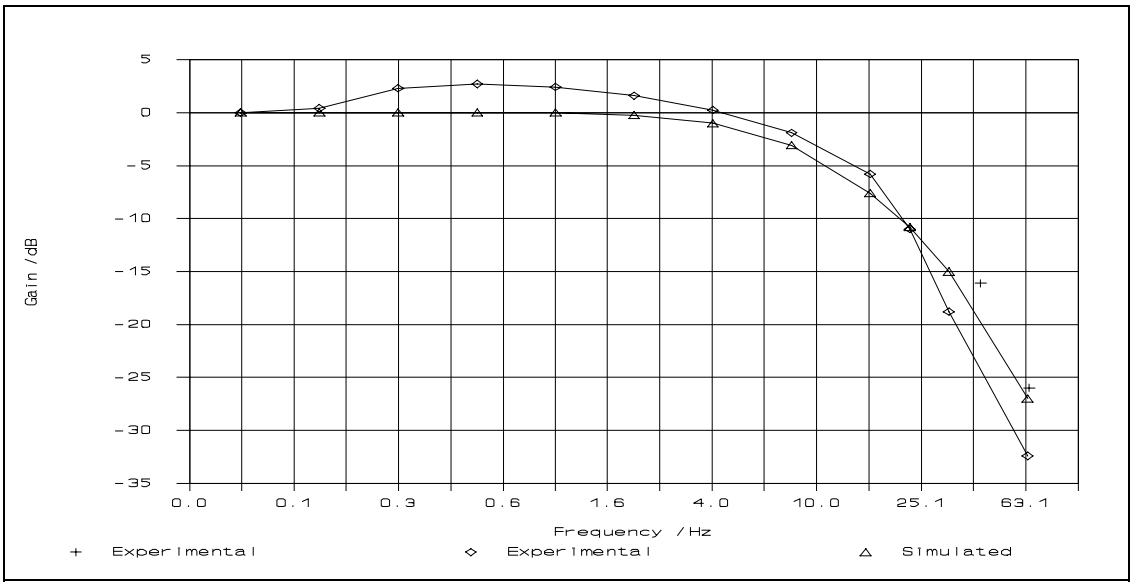

Figure 5.8 Bode plot (gain) for the position response of the heave mode suspension

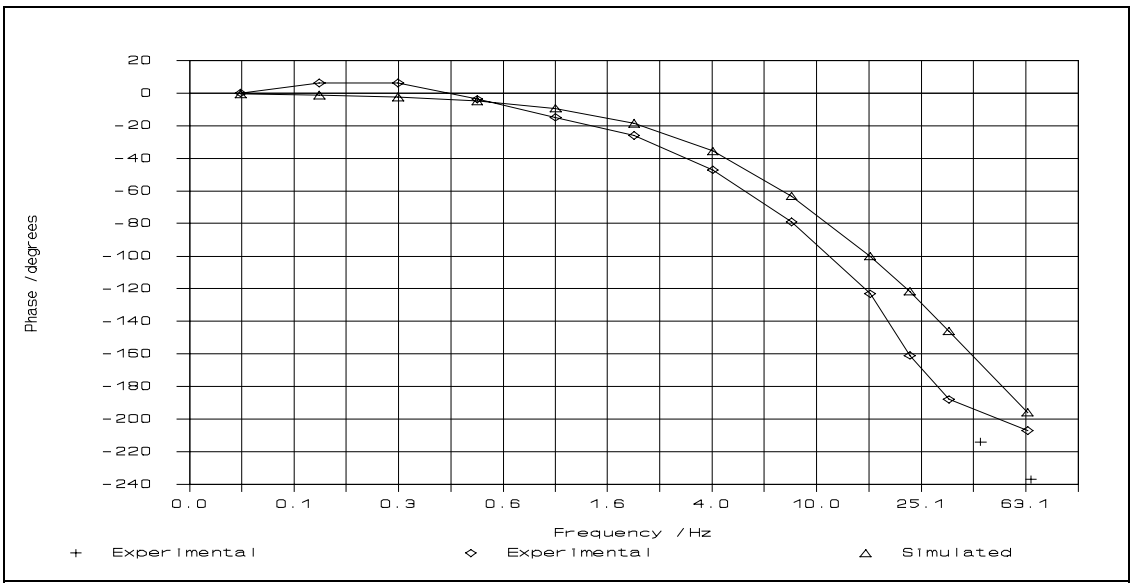

Figure 5.9 Bode plot (phase) for the position response of the heave mode suspension

In practice, the resonance characteristics of the electromagnet hangers and the track are a function of the proximity between the vehicle and the location of the guideway supports. The worst case vibration conditions were found experimentally and are marked on the Bode plots by the individual points measured at 42 Hz and 64 Hz. These are attributed to the track and electromagnet hangers for which the undamped natural frequencies were measured/estimated to be about 40 Hz and 70 Hz respectively. The theoretical Bode plots assume that the track is rigidly coupled to the ground.

The gain stability margin[84] for the experimental system is 17 dB compared with a theoretical value of 23 dB. This discrepancy is attributed to the neglection of discrete-time effects, and also to system model and implementation inaccuracies, in the theoretical value. The phase stability margin for the experimental system is about 130° versus a theoretical value which approaches 180°. This difference is mostly due to the state integration filters and position error integral action which are neglected in the theoretical calculation. The Bode plots clearly demonstrate a very good correspondence between the theory and the experimental results from the suspension system, and also that acceptable stability margins have been achieved.

The time and frequency domain responses for the other position controlled modes, namely pitch and roll, are dominantly the same as those for the heave mode, and so they are not presented here. However, the following two test phases present results which include some time domain responses for all of the vehicle modes.

5.6.2 Decoupling of the vehicle modes and load sharing

Having established a satisfactory performance from the vehicle mode controllers when tested independently, the cross-coupling between the different modes is now examined. Figure 5.10, Figure 5.11, Figure 5.12 show the responses of each vehicle mode to a 1 mm reference step input to the heave, pitch and roll position controllers respectively.

The cross-coupling of the heave, pitch and roll modes to the torsion mode is clearly negligible on all of the experimental test responses. The constant 0.1 mm torsion position offset reflects the fact that the vehicle chassis and track have a gap misalignment of +0.1 mm at one diagonal pair of electromagnets, and -0.1 mm at the other pair.

Low frequency cross-coupling after the transient portion of the step response is apparent between the heave, pitch and roll modes. This is caused by the electromagnet force controllers independently adjusting to their new operating points, and it results in a maximum coupling ratio of 8%. The only significant cross-coupling during the transient part of the step responses links the pitch to the heave mode, and the roll to the heave mode. This occurs because the centre of mass of the vehicle is above the horizontal plane on which the accelerometers are located, and it gives rise to a coupling ratio of 6%. The low amplitudes of the transient cross-coupling and the low frequency cross-coupling clearly illustrate the success of the proposed control strategy in terms of

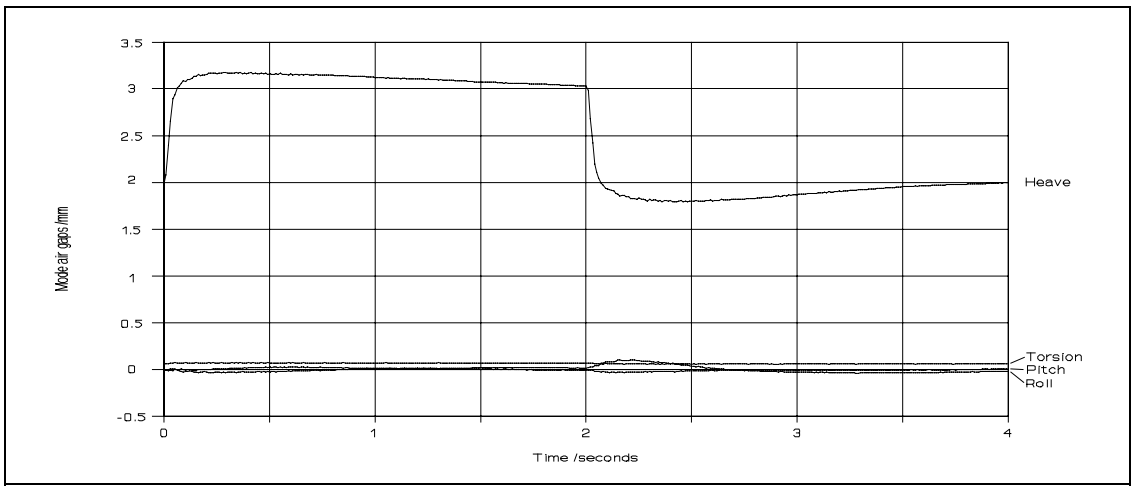

Figure 5.10 Experimental mode responses to a 1 mm *heave* position reference step

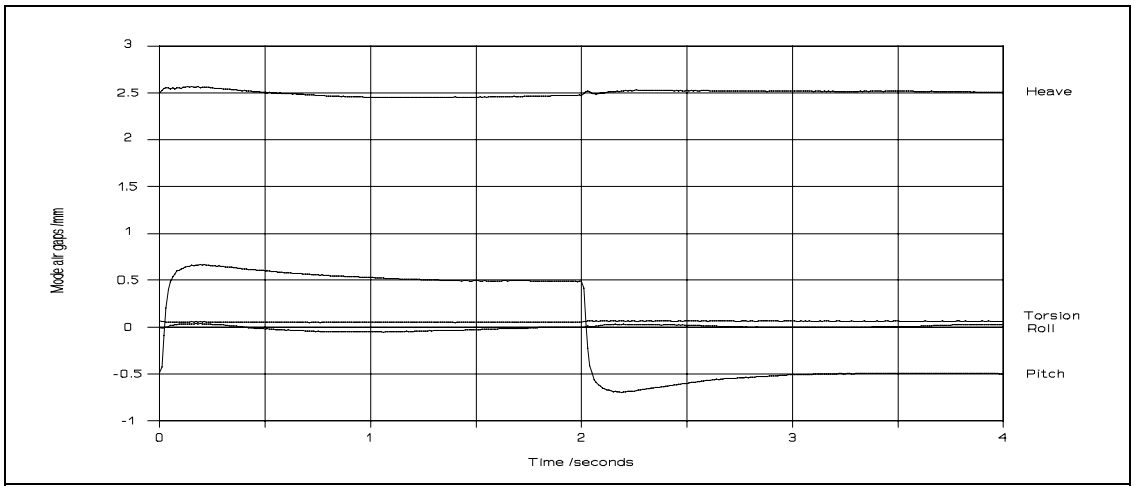

Figure 5.11 Experimental mode responses to a 1 mm *pitch* position reference step

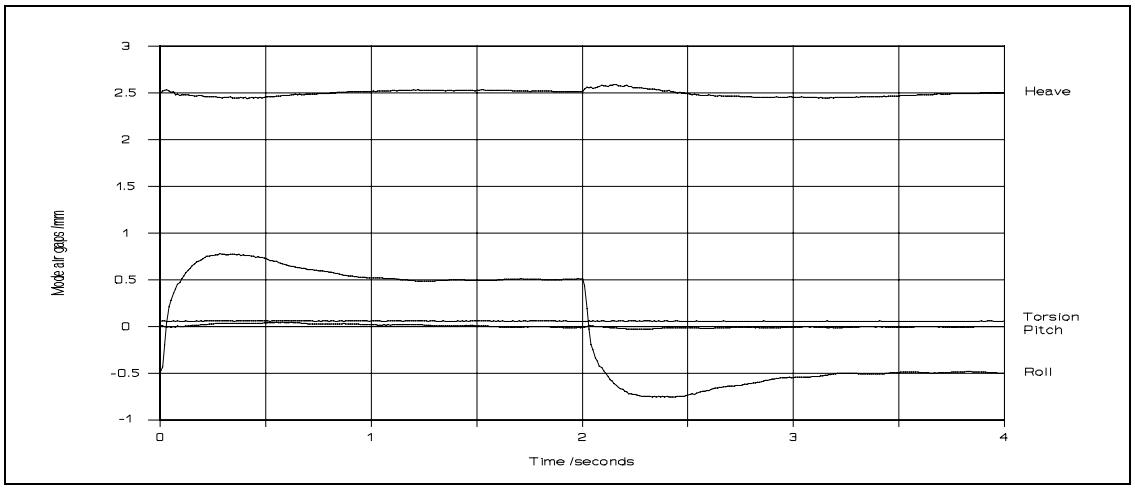

Figure 5.12 Experimental mode responses to a 1 mm *roll* position reference step

decoupling the vehicle mode motions.

The lightly damped roll oscillations generated by the roll step are attributed to a small cross-coupling to the lateral vehicle motion which is undamped. Finally, the very low amplitude, high frequency oscillation apparent on all of the mode responses is due to slight vibration of the electromagnet hangers as discussed in the previous test phase.

The load sharing capability of the vehicle suspension is tested by comparing the operating conditions of the electromagnets at the point on the experimental guideway where the torsional misalignment between the vehicle and guideway is at its maximum. Table 5.4 gives a snapshot of the worst case operating conditions at which each electromagnet deviates from its nominal value by approximately ±0.2 mm. The table is augmented with another snapshot of the control system, but this time it is reconfigured with the torsion position error, and error integral feedback gains set equal to the respective gains for the other vehicle modes. Such a suspension configuration is equivalent to using four independent electromagnet suspension controllers.

Table 5.4 Effects of worst case experimental vehicle to guideway misalignment

Parameter	**Electromagnets / Vehicle modes**			
Electromagnet air gaps (1,2,3,4) /mm	3.21	2.77	3.21	2.81
Vehicle mode gaps (h,p,r,t) /mm	3.00	0.01	-0.01	0.21
Electromagnet force demands /N	279	307	300	275
Electromagnet current demands /A	7.7	7.1	8.0	6.8
Electromagnet power dissipations /W	53	45	58	42
For controller with torsional position error plus integral feedback:				
Electromagnet force demands /N	567	20	602	27
Electromagnet current demands /A	10.8	1.8	11.2	2.2
Electromagnet power dissipations /W	105	3	113	4

The air gaps of diagonal pairs of electromagnets (see Figure 5.2) are approximately 2.8 mm and 3.2 mm, thus the larger air gaps are approximately 14% bigger than the smaller ones. The theoretical current ratio should therefore also be 14%, and the power

dissipation ratio 30%. In fact, due to a slightly uneven load distribution, the highest electromagnet power dissipation is 38% above the lowest.

The experimental data for the reconfigured suspension with effectively independent controllers shows that two of the electromagnets carry 96% of the vehicle load. Also, as the vehicle moves along the guideway, the torsion error changes, and this causes massive and rapid force fluctuations as the vehicle load is swapped between diagonal electromagnet pairs. This clearly demonstrates why such a configuration is unacceptable from both a steady-state and a dynamic viewpoint.

5.6.3 Ride quality of the vehicle suspension

The final test for the vehicle is for suspension ride quality whilst negotiating a step in track height. The experimental guideway does not have any track steps so they are simulated by injecting a step into the track position calculation. The experimental response to a 1 mm step change in track heave position is shown in Figure 5.13 for the unladen vehicle and in Figure 5.14 for the vehicle loaded with an 80 kg passenger. Comparison of the experimental responses with the simulated responses for the single electromagnet suspension (see Figure 4.11) shows that the experimental responses agree well with the theory. The peak acceleration is 0.025 g which is comfortably below the ISO target of 0.04 g. The low frequency overshoot (approximately 25%) is again due to the a.c. coupling of the feedback signals derived from the accelerometers.

Figure 5.15, Figure 5.16, Figure 5.17 show the experimental responses for a 2 mm simulated track position step for the heave, pitch and roll modes. These show that a dominantly consistent response is obtained for each of the vehicle modes. The pitch response overshoot is 16% which is approximately equal to that attributed to the a.c. coupling of the velocity and position feedback signals (see Section 4.4.6). The heave response has an additional, slower contribution due to error integral action as the electromagnet force controllers adjust to the new operating point.

Finally, the roll response overshoot, at 29%, is 13% higher than that of the pitch mode. Cross-coupling of the roll mode to the undamped sway mode was observed during the track step response test, and the additional roll mode overshoot is attributed to this cross-coupling. The cross-coupling occurs because the centre of mass of the vehicle is located above the plane on which the accelerometers are located. Active control of

the lateral vehicle modes should reduce the roll mode overshoot to a similar level to that experienced by the pitch mode.

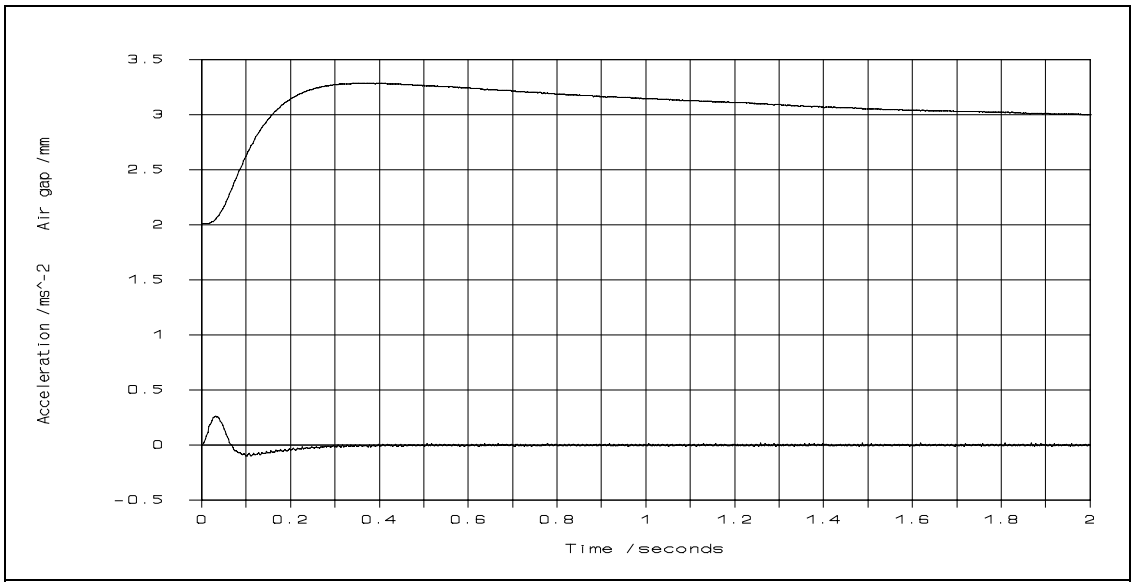

Figure 5.13 Experimental heave response to a 1 mm simulated track step (no passenger)

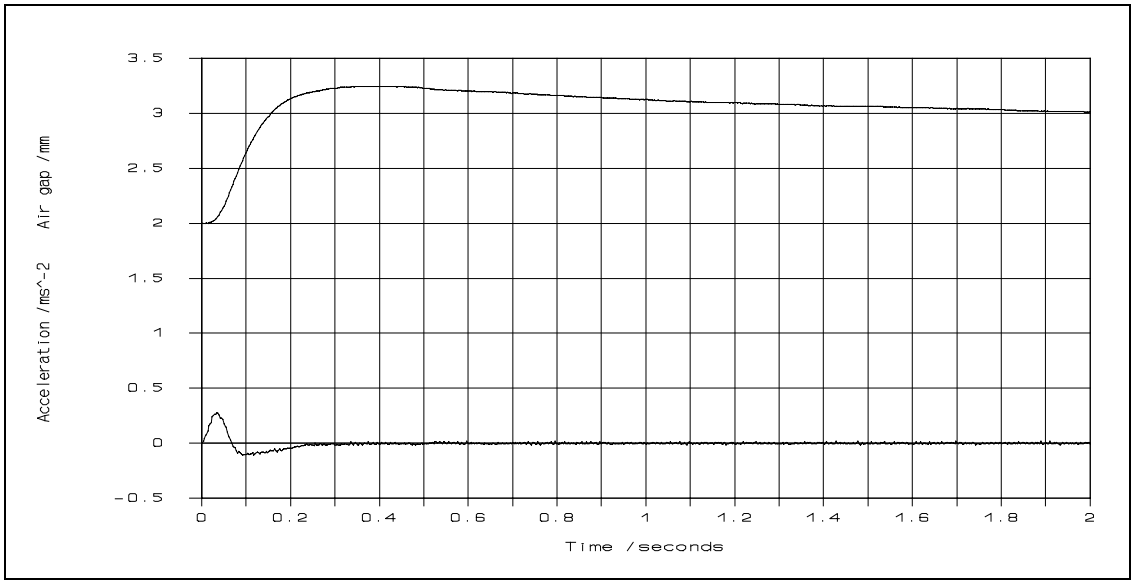

Figure 5.14 Experimental heave response to a 1 mm simulated track step (80 kg passenger)

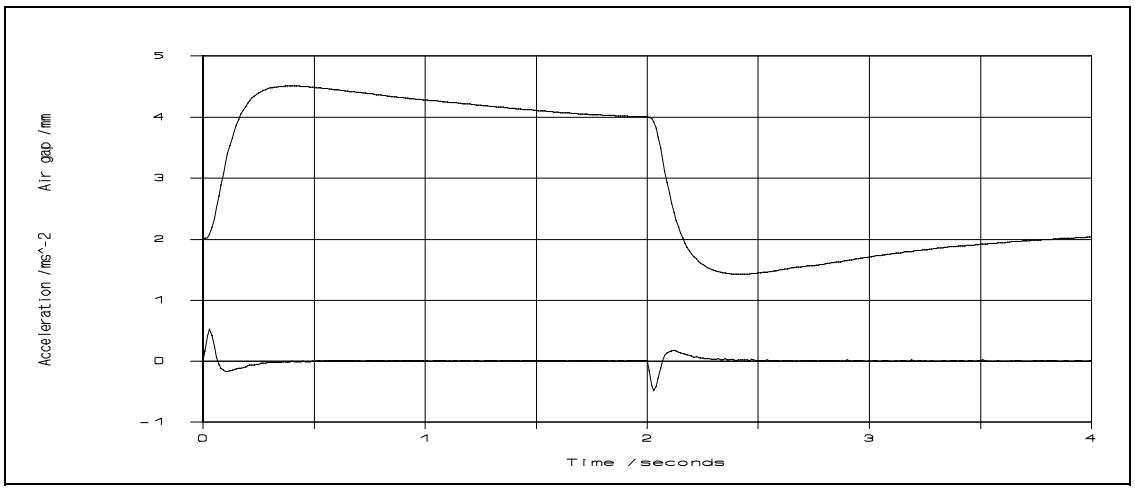

Figure 5.15 Experimental heave response to a 2 mm simulated track *heave* step

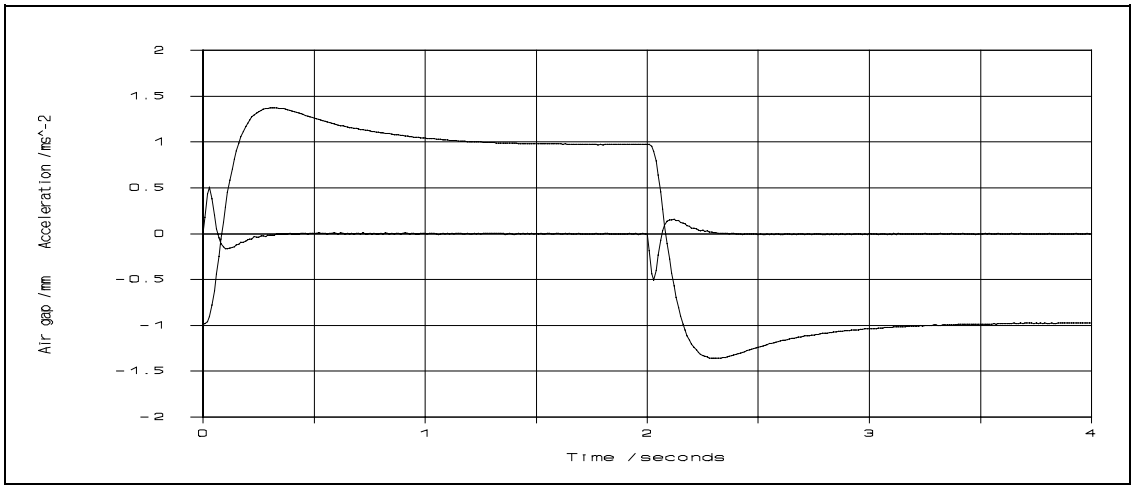

Figure 5.16 Experimental pitch response to a 2 mm simulated track *pitch* step

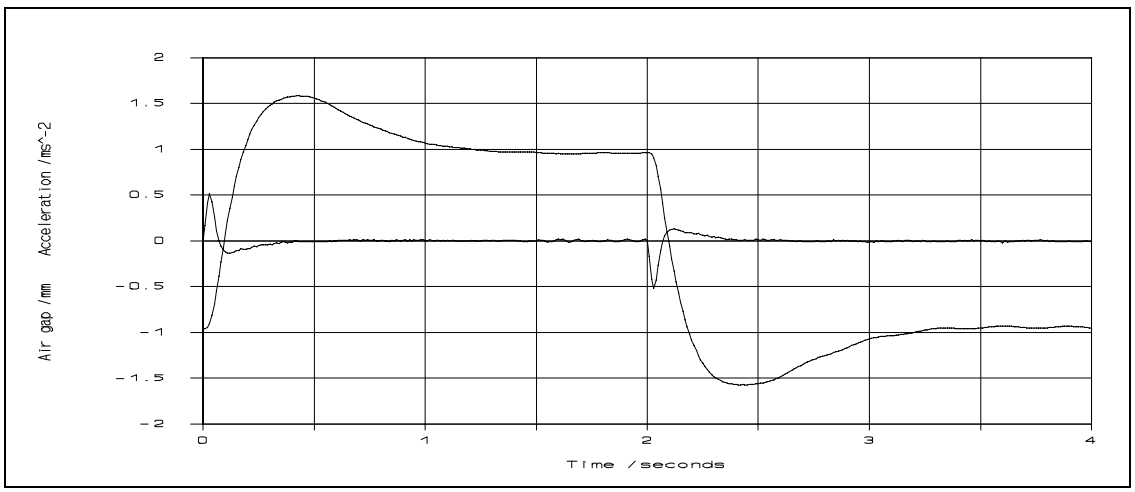

Figure 5.17 Experimental roll response to a 2 mm simulated track *roll* step

5.7 Conclusions

This chapter describes the development and validation of the multi-electromagnet vehicle suspension control strategy outlined in Chapter 1. The experimental system achieved a very good performance in terms of passenger ride quality, disturbance force rejection, and electromagnet utilisation. The last feature arises from the ability of the proposed control strategy to support the use of position error integral action which facilitates accurate control of the nominal air gaps and hence maximises the available air gap deviations. These benefits accrue from the development of a detailed electromagnet model for the force control algorithm, and a sophisticated structure for the vehicle suspension control system.

Finally, it is apparent that existing vehicle control strategies require detailed consideration of the nonlinear force actuators throughout the design procedure in order to get predictable results.[85] By contrast, the linearity of the proposed electromagnet force controller permits the assumption of linear force actuation. This fact, coupled with the modularity of the proposed suspension control strategy, permits a linear vehicle suspension design procedure, which consists of decoupling the electromagnet motions and then configuring the mode suspension controllers.